Effects of Beam Patterns on Removal of Phosphorous in Silicon by Electron Beam Melting

Shuang Shi, Yi Tan, Dachuan Jiang, Wei Dong, Shutao Wen

A heat transfer model for Si refining by electron beam melting is proposed to obtain the temperature distribution of the molten Si. The results show that the temperature distribution is extremely inhomogeneous, especially on the molten surface. Based on the temperature distribution, the evaporation rates of P and Si are also discussed and the corresponding experiment was carried out to be compared with the theoretical calculation. The results show that the evaporation rates of P and Si reduce and the ratio of the evaporation rate of P to Si increases with the increasing of the electron beam pattern radius. A critical molten pool with a large surface area exists when the pattern radius reaches to a certain value, which is considered to be the optimal pattern radius due to a relatively high removal efficiency of P and a low loss efficiency of Si.

Влияние на лъча върху отстраняването на фосфор в силиций чрез електроннолъчево топене (С. Ши, И. Тан, Д. Жианг, У. Донг, С. Уен). *Предложен е модел за топлопренасянето при рафиниране на силиций за получаване на температурното разпределение на разтопения силиций. Резултатите показват, че температурното разпределение е изключително нехомогенно, особено на разтопената повърхност. На база на температурното разпределение са дискутирани също скоростите на изпарение на фосфор и силиций и е проведен съответстващ експеримент за сравнение с теоретичните изчисления. Резултатите показват, че скоростите на изпарение на фосфор и силиций намаляват и отношението на скоростта на изпарение на фосфор към тази на силиций се увеличава с увеличаване на радиуса на лъча. Съществува критична течна вана с голяма повърхност, когато радиуса стига до определена стойност, който се приема за оптимален радиус, благодарение на сравнително голямата ефективност на отстраняване на фосфор и на малките загуби на силиций.*

Introduction

In recent years, the requirement for solar-grade silicon increases dramatically with the rapid development of the photovoltaic industry[1-3]. As one of the major impurities, P deteriorates the electrical properties of silicon materials, such as electrical resistivity and minority carrier lifetime. Therefore, it needs to be removed to less than 1×10^{-5} wt.%, to meet the performance requirement of solar cells.

Electron beam melting has been applied in purification of Si materials, which has been proved to be an effective method to remove volatile impurities[4-9]. During electron beam melting process, pattern radius, defined as the radius of electron beam scanning track, is an important factor that affects the state of the molten pool. Different pattern radiuses lead to different temperature and surface area at a certain power, so as to influence the evaporation rate. However, the surface temperature of the molten pool is difficult to measure directly due to the characteristic of local high energy of electron beam melting, which is always roughly calculated by the loss of Si. So far, only few reports on the temperature distribution of the molten pool and the corresponding removal rate of P during electron beam melting are available to date.

In this paper, a model for Si refining by electron beam melting is proposed to obtain the temperature distribution in the molten silicon, especially on the surface of the molten pool. Based on the results, the evaporation rates of P and Si are also calculated to evaluate the removal efficiency of P and the loss of Si. Moreover, the optimal pattern radius at a certain electron beam power is discussed.

Mathematical model development

A cylindrical ingot is considered in the mathematical model to obtain the temperature

distribution on the silicon ingot during electron beam melting, as shown in Fig. 1. The bottom of the ingot contacts directly to a water-cooled copper crucible. As a heat source, the electron beam irradiates the top surface of the ingot in a circular trajectory.

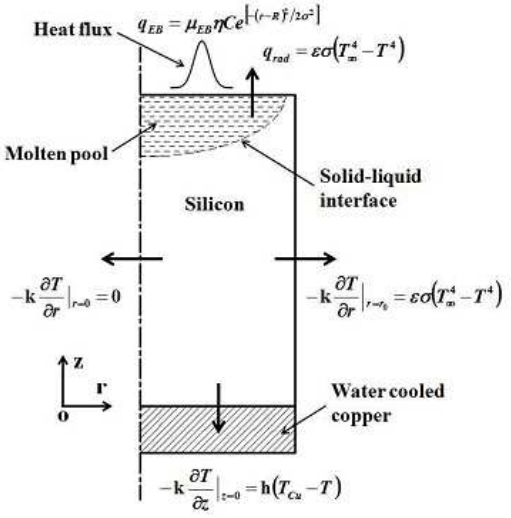

Fig.1. Schematic illustration of the mathematical model

A heat transfer model is developed according to the following assumptions:

(a) The geometry of the model configuration is axisymmetric;

(b) Heat transfer occurs only along the axial and radial directions;

(c) The thermal and physical properties of the material are independent of time.

The heat flow in the radial direction, *r*, and in the axial direction, *z*, can be described by heat conduction equation as follows:

$$\rho C_P \frac{\partial T}{\partial t}=\frac{1}{r}\frac{\partial}{\partial r}\left(kr\frac{\partial T}{\partial r}\right)+\frac{\partial}{\partial z}\left(k\frac{\partial T}{\partial z}\right)+Q \quad (1)$$

where T (K) is the temperature, t (s) is the melting time, r (m) is the radius, z (m) is the axial height, ρ (g m^{-3}) is the density, C_p (J kg^{-1} K^{-1}) is the specific heat, k (W m^{-1} K^{-1}) is the thermal conductivity, and Q (W m^{-3}) is the volumetric latent heat associated with the phase transformation. The input heat flux from the electron beam, q_{EB} (W m^{-2}) can be described by a normal distribution function[10]:

$$q_{EB}=\mu_{EB}\eta C\exp[-(r-R)^2/2\sigma^2] \quad (2)$$

where μ_{EB} is the electron beam power transfer efficiency, η is the normalized electron beam power, C (W m^{-2}) is a pre-exponential constant, r (m) is the radius, R (m) is the center position of the beam pattern, and σ (m) is the standard deviation of the distribution.

For the calculation, the initial temperature of the ingot is set to 298 K. Since the copper crucible is far from the heat source, the temperature of the environment and the copper crucible are set to 298 K, respectively. The validity of this assumption is confirmed by the absence of temperature change in the water inlet and outlet of the crucible during refining.

The boundary conditions are given as follows:

On the top surface of the ingot, the net heat flux consists of two parts, the electron beam energy density, q_{EB} (W m^{-2}), and the surface heat irradiation flux, q_{rad} (W m^{-2}):

$$-k\left.\frac{\partial T}{\partial z}\right|_{z=z_0}=q_{EB}+q_{rad} \quad (3)$$

The surface heat irradiation flux can be expressed as

$$q_{rad}=\varepsilon\sigma\left(T_\infty^4-T^4\right) \quad (4)$$

where ε is the emissivity of the Si surface, σ (5.67 × 10^{-8} W m^{-2} K^{-1}) is the Stephan-Boltzmann constant, and T_∞ (K) is the far-field temperature.

On the bottom surface of the ingot:

$$-k\left.\frac{\partial T}{\partial z}\right|_{z=0}=h\left(T_{Cu}-T\right) \quad (5)$$

where h (W m^{-2} K^{-1}) is the heat transfer coefficient and T_{Cu} (K) is the temperature of the water-cooled copper crucible.

On the outside surface of the ingot:

$$-k\left.\frac{\partial T}{\partial r}\right|_{r=r_0}=\varepsilon\sigma\left(T_\infty^4-T^4\right) \quad (6)$$

Based on the above boundary conditions, the temperature distribution in the vertical cross-section of the ingot during electron beam melting can be calculated.

Results and discussion

Temperature distribution

Two ingots with a same ratio of radius to height are calculated by the aforementioned model at a power of 6 kW. The typical steady state temperature distributions of the ingot cross-section are shown in Fig. 2.

Great temperature gradient exists in the axial direction of the ingot, which results from the heating on the top surface by the electron beam and the cooling on the bottom surface by the water-cooled

copper crucible. However, the temperature gradients in the radial direction are different along the height of the ingot. The area directly irradiated by the electron beam is within the range of the highest temperature due to high energy density input. With continuous irradiation by electron beam, heat energy transfers from the area to the surroundings. So the upper part of the ingot shows a great temperature gradient in the radial direction, especially on the top surface. In contrast, the bottom part of the ingot shows no temperature gradient in the radial direction.

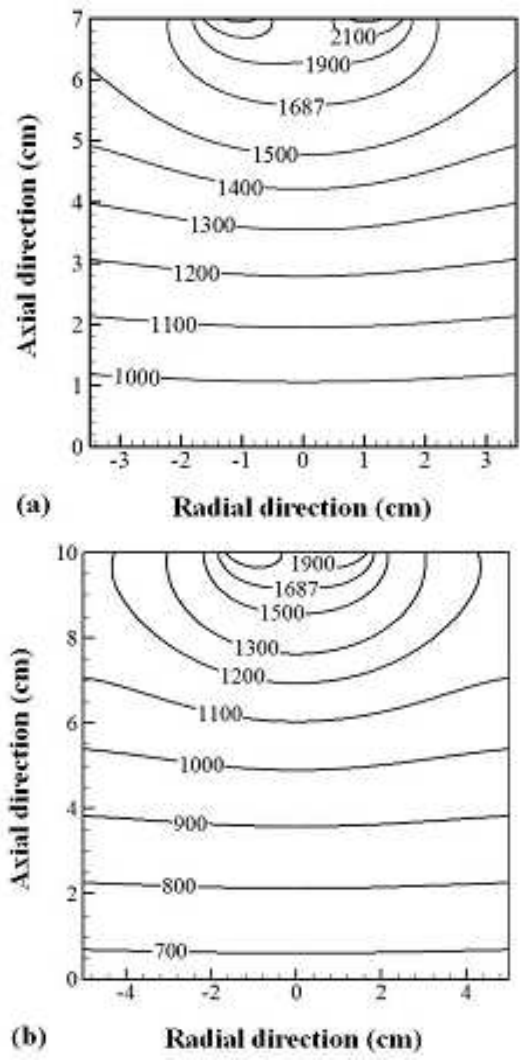

Fig.2. Temperature distributions on the cross-section of the ingots (left: radius 3.5cm, height 7cm; right: radius 5cm, height 10cm)

Change of pattern radius leads to a variation of the temperature distribution on the surface. Figure 3 shows five typical temperature distributions on the surface of the ingot with different pattern radiuses.

A peak shaped temperature distribution is formed with a high temperature in the central part and a low temperature in the surrounding when the pattern radius is small, due to the relatively concentrated energy in the center nearby. With the pattern radius increases, the temperature of the central part decreases, and the peak value of the temperature moves peripheral so that an annular peak of temperature distribution is formed.

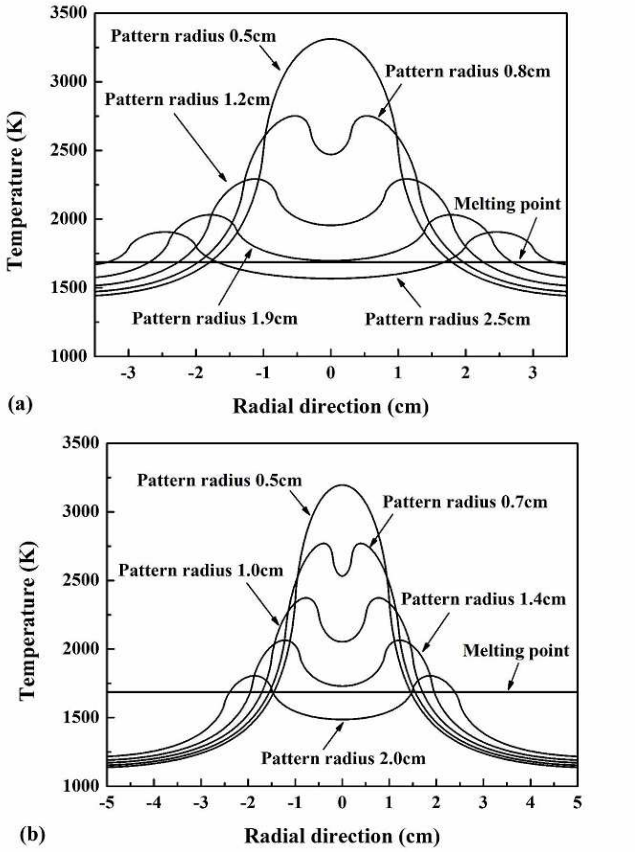

Fig. 3. Temperature distributions on the surface of the ingots (left: radius 3.5cm, height 7cm; right: radius 5cm, height 10cm)

The temperature of the surface centre will reduce to the melting point when the pattern radius increases continually to a certain value. The molten pool in this state is called the critical molten pool and the patter radius is defined as the critical patter radius. If the pattern radius is larger than the critical value, the central part of the ingot doesn't melt because the temperature is less than the melting point.

Characteristics of the molten pool

According to temperature distribution on the ingot surface, the surface area of the molten pool can be calculated, as shown in Fig.4.

A molten pool with a small surface area forms due to a relatively concentrated energy when the pattern radius is small. As the pattern radius increases, the surface area of the molten pool enlarges due to a

relatively decentralized energy until a critical molten pool forms. At this moment, the surface area of the molten pool approximates to its maximum. The variation trends of the surface area are different for the two ingots when the pattern radius is more than the critical value.

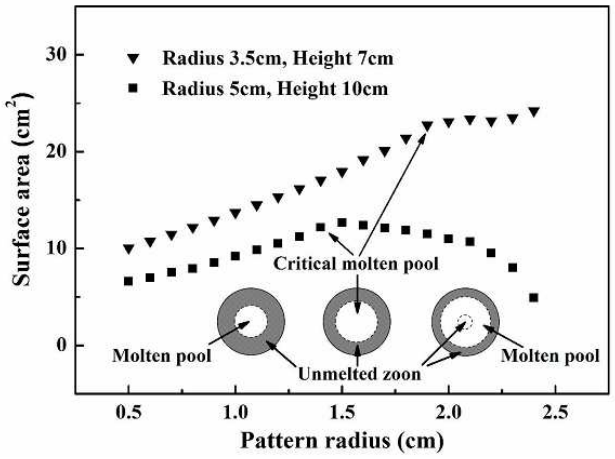

Fig. 4. The surface area of the molten pool with different pattern radiuses

As for the ingot with a radius of 5 cm and a height of 10 cm, the surface area continues to enlarge to maximum when the pattern radius is just over the critical value, but the unmelted area has formed in the center. After that, the surface area reduces until there is no area being melted. As for the ingot with a radius of 3.5 cm and a height of 7 cm, the surface area stays in a range when the pattern radius is larger than the critical value, and the edge of the top surface will be melted if it is over 2.4 cm. The different trends for the two ingots stem from the dimension effect. At a constant power, the melting capacity of the electron beam is limited. For the larger ingot, electron beam with a large pattern radius cannot provide enough energy so that the surface area of the molten pool reduces until it disappears. For the smaller one, when the pattern radius is more than the critical value, the border of the molten pool is closed to the edge of the ingot, leading to a change of the heat transmission condition.

Analysis of phosphorous removal and loss of Si

The rate of idea evaporation in unit area of P into vacuum W_P (kg m^{-2} s^{-1}) varies with temperature can be expressed by[11]

$$W_P = P_{atm} f_P C_P \exp\left(-\frac{\Delta G^0}{RT}\right)\sqrt{\frac{M_P}{2\pi RT}} \quad (7)$$

where T (K) is the absolute temperature, R (8.3154 J mol^{-1} K^{-1}) is the gas constant, K is the equilibrium constant, P_P (Pa) is the partial vapor pressure of P over molten silicon, P_{atm} (101325 Pa) is the atmosphere pressure, f_P is Henry activity coefficient of P related to 1 wt pct in an infinitely dilute solution, C_P (%) is the mass fraction, M_P (0.031 kg mol^{-1}) is the molar mass of P.

The mathematical model is developed base on the assumption that the geometry of the model configuration is axisymmetric, so the surface temperature of the molten pool can be regarded as a function of the radius, i.e. *T(r)*. The total rate of idea evaporation of P, W_{total} (kg s^{-1}) can be obtained by integration from zero to the whole surface area of the molten pool:

$$W_{total} = \iint_S W_P dS \quad (8)$$

In the process of removing P from Si, the matrix can evaporate in a high temperature and vacuum condition, so the loss of Si is also investigated. The rate of idea evaporation in unit area of Si into vacuum V_{Si} (kg m^{-2} s^{-1}) is obtained by Hertz-Knudsen-Langmuir equation[12]:

$$V_{Si} = P_{Si}^0 \cdot \sqrt{\frac{M_{Si}}{2\pi RT}} \quad (9)$$

where P_{Si}^0 (Pa) is the vapor pressure above the melt of pure Si, M_{Si} (0.028 kg mol^{-1}) is the molar mass of Si, R is the gas constant, and T (K) is the absolute temperature of the surface. The vapor pressure of pure Si can be expressed by:

$$\log P_{Si}^0 = AT^{-1} + B\log T + CT + D \quad (10)$$

where A, B, C and D are constants which can be found in thermodynamics data base. According to equation (12) and (13), the total evaporate rate of Si V_{total} (kg s^{-1}) can be obtained integration from zero to the whole surface area of the molten pool:

$$V_{total} = \iint_S V_{Si} dS \quad (11)$$

Figure 5 shows the theoretical and experimental results of the evaporation rates of P and Si as a function of pattern radius. The experimental value is obtained from A Si ingot with the dimension of 70 × 58 × 73 mm3, the area of the top surface of which is approximate equal to that of a cylindrical ingot with a radius of 3.5 cm and a height of 7 cm used in the theoretical calculation. The initial content of P in the ingot was 1.44 × 10^{-2} wt.%. As the pattern radius increases, the evaporation rates of both P and Si show a downward trend. The reason is that the surface

temperature of the molten pool reduces due to energy dispersion with a large beam pattern. The experimental values are consistent with the theoretical value in the range of permitted errors.

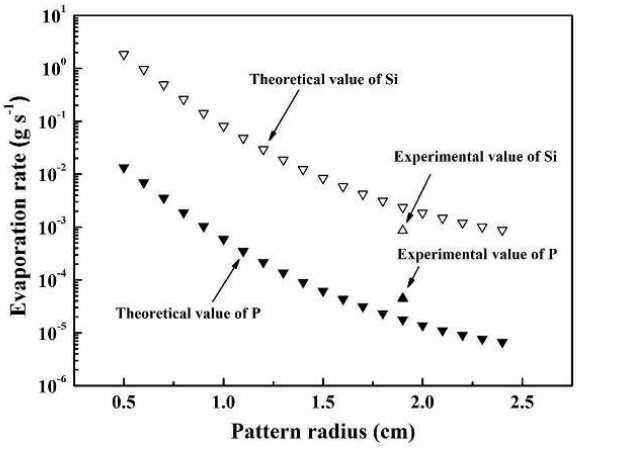

Fig. 5. The evaporation rate of P and Si with different pattern radiuses

During electron beam melting process, P needs to be removed and Si needs to be reserved, so the ratio of evaporation rates of P to Si is also calculated. A small pattern radius leading to a high surface temperature is beneficial to the removal of P, but in this case, the loss of Si is also large. On the contrary, a large pattern radius can reduce the loss of Si, but when it is more than the critical value, a circular molten pool forms on the top of the ingot with the center part being unmelted. In consideration of the above factors, the critical molten pool with a large surface area is considered to be the optimal electron beam pattern radius during electron beam melting with a constant power.

However, it should be noted that all of the calculations are discussed in ideal conditions. In fact, the residual chamber pressure is comparable to the vapor pressure of evaporating species, so collisions between evaporant atoms and residual gas molecules or evaporant atoms themselves may change the evaporation rate by a small amount.

Conclusion

According to the temperature distribution in the molten pool based on a heat transfer model, the evaporation rates of P and Si during Si refining processing by electron beam melting is discussed. As the pattern radius increases, the evaporation rates of P and Si reduce, but the ratio of the evaporation rate of P to Si increases. There exists a critical molten pool when the pattern radius reaches a certain value. At this time, impurity P can be removed effectively and the evaporation rate of Si is in a low level, leading to a relatively high removal efficiency of P and a low loss efficiency of Si.

Acknowledgements

The author gratefully acknowledges financial support from National Key Technology R & D Program (Grant No. 2011BAE03B01) and the Natural Science Foundation of China (Grant No. U1137601).

REFERENCES

[1] T. Schutz-Kuchly, V. Sanzone, Y. Veschetti, N-type solar-grade silicon purified via the metallurgical route: characterisation and fabrication of solar cells, Prog. Photovoltaics, 2013, 21, 1214.

[2] F. Tanay, S. Dubois, N. Enjalbert, J. Veirman, Low temperature-coefficient for solar cells processed from solar-grade silicon purified by metallurgical route, Prog. Photovoltaics, 2011, 19, 966.

[3] M.A. Martorano, J.B. Ferreira Neto, T.S. Oliveira, T.O. Tsubaki, Refining of metallurgical silicon by directional solidification, Mater. Sci. Eng. B, 2011, 176, 217.

[4] D.C. Jiang, S. Shi, Y. Tan, D.Y. Pang, W. Dong, Research on distribution of aluminum in electron beam melted silicon ingot, Vacuum, 2013, 96, 27.

[5] Y. Tan, S.T. Wen, S. Shi, D.C. Jiang, W. Dong, X.L. Guo, Numerical simulation for parameter optimization of silicon purification by electron beam melting, Vacuum, 2013, 95, 18.

[6] S. Shi, W. Dong, X. Peng, D.C. Jiang, Y. Tan, Evaporation and removal mechanism of phosphorus from the surface of silicon melt during electron beam melting, Applied Surface Science, 2013, 266, 344.

[7] Y. Tan, X.L. Guo, S. Shi, W. Dong, D.C. Jiang, Study on the removal process of phosphorus from silicon by electron beam melting, Vacuum, 2013, 93, 65.

[8] Q. Wang, W. Dong, Y. Tan, D.C. Jiang, C. Zhang and X. Peng: Impurities evaporation from metallurgical-grade silicon in electron beam melting process, Rare Metals, 2011, 30, 274.

[9] X. Peng, W. Dong, Y. Tan and D.C. Jiang: Removal of aluminum from metallurgical grade silicon using electron beam melting, Vacuum, 2011, 86, 471.

[10] D.M. Maijer, T. Ikeda, S.L. Cockcroft, M. Maeda and R.B. Rogge: Mathematical modeling of residual stress formation in electron beam remelting and refining of scrap silicon for the production of solar-grade silicon, Mater. Sci. Eng. B, 2005, 390, 188.

[11] T. Miki, K. Morita and N. Sano: Thermodynamics of phosphorus in molten silicon, Metall. Mater. Trans. B, 1996, 27B, 937.

[12] O.E. Shklyaev and E. Fried: Stability of an evaporating thin liquid film, J Fluid Mech., 2007, 584, 157.

Dr. S. Shi *- School of Materials Science and Engineering, Dalian University of Technology, No. 2 Linggong Road, Ganjingzi District, Dalian 116023, China.*

tel.:+86 411 84709784 e-mail: shishuang1217@163.com

Prof. Y. Tan *- School of Materials Science and Engineering, Dalian University of Technology, No. 2 Linggong Road, Ganjingzi District, Dalian 116023, China.*

tel.:+86 411 84707583 e-mail: tanyi@dlut.edu.cn

Dr. D. C. Jiang *- School of Materials Science and Engineering, Dalian University of Technology, No. 2 Linggong Road, Ganjingzi District, Dalian 116023, China.*

tel.:+86 411 84709784 e-mail: cipjjs@126.com

Assoc. Prof. W. Dong *- School of Materials Science and Engineering, Dalian University of Technology, No. 2 Linggong Road, Ganjingzi District, Dalian 116023, China.*

tel.:+86 411 84707455 e-mail: w-dong@dlut.edu.cn

Dr. S. T. Wen *- School of Materials Science and Engineering, Dalian University of Technology, No. 2 Linggong Road, Ganjingzi District, Dalian 116023, China.*

tel.:+86 411 84709784 e-mail: wenshutao.170@126.com